J|A|C|S
ARTICLES
Published on Web 02/19/2002

Searching for the Second Oxidant in the Catalytic Cycle of Cytochrome P450: A Theoretical Investigation of the Iron(III)-Hydroperoxo Species and Its Epoxidation Pathways

François Ogliaro, Sam P. de Visser, Shimrit Cohen, Pankaz K. Sharma, and Sason Shaik*

Contribution from the Department of Organic Chemistry and the Lise Meitner-Minerva Center for Computational Quantum Chemistry, Hebrew University, 91904, Jerusalem

Received September 29, 2001

Abstract: Iron(III)-hydroperoxo, [Por(CysS)Fe(III)-OOH]$^-$, a key species in the catalytic cycle of cytochrome P450, was recently identified by EPR/ENDOR spectroscopies (Davydov, R.; Makris, T. M.; Kofman, V.; Werst, D. E.; Sligar, S. G.; Hoffman, B. M. *J. Am. Chem. Soc.* **2001**, *123*, 1403−1415). It constitutes the last station of the preparative steps of the enzyme before oxidation of an organic compound and is implicated as the second oxidant capable of olefin epoxidation (Vaz, A. D. N.; McGinnity, D. F.; Coon, M. J. *Proc. Natl. Acad. Sci. U.S.A.* **1998**, *95*, 3555−3560), in addition to the penultimate active species, Compound I (Groves, J. T.; Han, Y.-Z. In *Cytochrome P450: Structure, Mechanism and Biochemistry*, 2nd ed.; Ortiz de Montellano, P. R., Ed.; Plenum Press: New York, 1995; pp 3−48). In response, we present a density functional study of a model species and its ethylene epoxidation pathways. The study characterizes a variety of properties of iron(III)-hydroperoxo, such as the O−O bonding, the Fe−S bonding, Fe−O and Fe−S stretching frequencies, its electron attachment, and ionization energies. Wherever possible these properties are compared with those of Compound I. The proton affinities for protonation on the proximal and distal oxygen atoms of iron(III)-hydroperoxo, and the effect of the thiolate ligand thereof, are determined. In accordance with previous results (Harris, D. L.; Loew, G. H. *J. Am. Chem. Soc.* **1998**, *120*, 8941−8948), iron(III)-hydroperoxo is a strong base (as compared with water), and its distal protonation leads to a barrier-free formation of Compound I. The origins of this barrier-free process are discussed using a valence bond approach. It is shown that the presence of the thiolate is essential for this process, in line with the "push effect" deduced by experimentalists (Sono, M.; Roach, M. P.; Coulter, E. D.; Dawson, J. H. *Chem. Rev.* **1996**, *96*, 2841−2887). Finally, four epoxidation pathways of iron(III)-hydroxperoxo are located, in which the species transfers oxygen to ethylene either from the proximal or from the distal sites, in both concerted and stepwise manners. The barriers for the four mechanisms are 37−53 kcal/mol, in comparison with 14 kcal/mol for epoxidation by Compound I. It is therefore concluded that iron(III)-hydroperoxo, as such, cannot be a second oxidant, in line with its significant basicity and poor electron-accepting capability. Possible versions of a second oxidant are discussed.

I. Introduction

Cytochrome P450 constitutes a superfamily of enzymes, which activate dioxygen and carry out monooxygenation processes of a variety of endogenous and xenobiotic compounds. The importance of these processes for life has presented an exciting agenda for research aimed at the elucidation of the monooxygenation mechanisms and the identification of the intermediate species in the catalytic cycle of the enzyme.[1] The most commonly accepted catalytic cycle[1−7] is shown in Figure 1 where the boxed area represents the "great unknowns", which are the nature of the active species and the mechanism of monooxygenation.

Until recently, a consensus seemed to have been reached that the active monooxygenating species of the enzyme is the high-valent oxoiron(IV) species, so-called compound I (Cpd I) and shown as **1** in Figure 1. Let us refer to this as the "single-oxidant hypothesis". Indeed, many mimetic Cpd I species have been made and used throughout the years to successfully perform hydroxylation and epoxidation reactions,[2,4−8] thereby buttressing the status of Cpd I as a potent oxidant. Nevertheless, this consensus was always clouded by the mere fact that Cpd I of P450 could not be observed, since it does not accumulate during

(1) Ortiz de Montellano, P. R., Ed. *Cytochrome P450: Structure, Mechanism and Biochemistry*, 2nd ed.; Plenum Press: New York, 1995.
(2) Sono, M.; Roach, M. P.; Coulter, E. D.; Dawson J. H. *Chem. Rev.* **1996**, *96*, 2841−2887.
(3) Davydov, R.; Makris, T. M.; Kofman, V.; Werst, D. E.; Sligar, S. G.; Hoffman, B. M. *J. Am. Chem. Soc.* **2001**, *123*, 1403−1415.
(4) Dawson, J. H. *Science* **1988**, *240*, 433−439.
(5) Dawson, J. H.; Sono, M. *Chem. Rev.* **1987**, *87*, 1255−1276.
(6) Woggon, W.-D. *Top. Curr. Chem.* **1996**, *184*, 39−95.
(7) Groves, J. T.; Han, Y.-Z. In *Cytochrome P450: Structure, Mechanism and Biochemistry*, 2nd ed.; Ortiz de Montellano, P. R. Ed.; Plenum Press: New York, 1995; pp 3−48.
(8) Meunier, B. *Chem. Rev.* **1992**, *92*, 1411−1456.

10.1021/ja0171963 CCC: $22.00

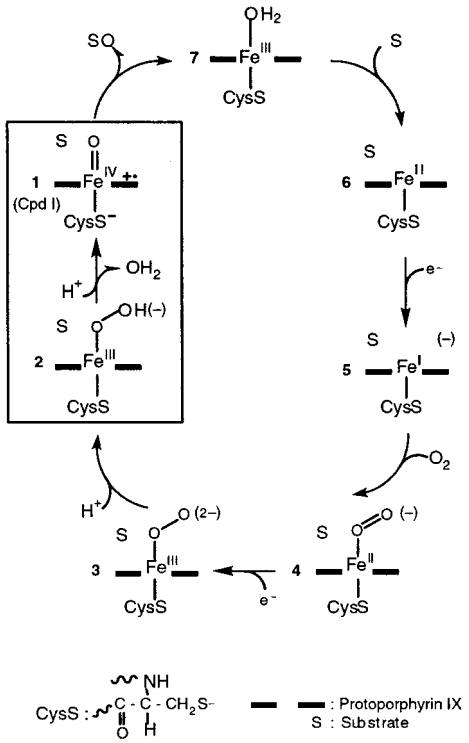

Figure 1. A catalytic cycle of cytochrome P450 (see ref 3).

the catalytic cycle. Exciting reports of such an observation by means of rapid scan spectroscopy[9] and cryogenic X-ray diffraction[10] were cast lately in doubt by an EPR/ENDOR study of the cryogenically generated intermediates in the catalytic cycle of the enzyme $P450_{cam}$.[3] This latter study identifies the iron(III)-hydroperoxo species, **2** in Figure 1, as the last station beyond which only the hydroxy-camphor product could be observed. However, analysis of the product showed that the monooxygenation leads to the iron(III)-hydroxy-camphor complex rather than to the resting state (**7**, Figure 1). Proton inventory analysis in the product complex showed that the C-5 hydrogen of camphor is trapped in the hydroxyl group of hydroxy-camphor. These facts seemed to be more consistent with monooxygenation of camphor by Cpd I (**1**) rather than by the iron(III)-hydroperoxo species (**2**). Nevertheless, the identity of the oxidant species (for substrates other than camphor) remains a nagging question: Is it Cpd I, **1**, or could it also be the iron(III)-hydroperoxo species, **2**?

The importance of **2** as a "second oxidant" in the cycle has been on the rise ever since Coon et al.[11−15] demonstrated that yet another species in the catalytic cycle, the iron(III)-peroxo species **3** (Figure 1) causes oxidative deformylation of aldehydes along with related reactions (aromatization). In a series of

Scheme 1. (a) Oxidant Species and Their Roles. (b) Probe Substrate for Cationic Species and the Proposed Role of **2**

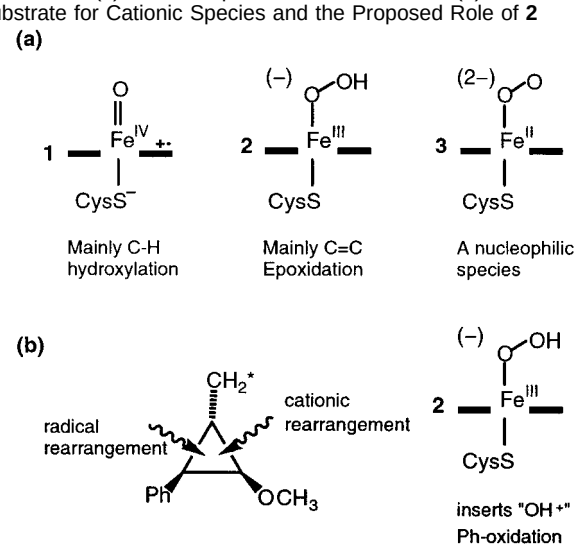

elegant mutations (replacing threonine, T, by alanine, A) which affect the proton delivery that converts **2** to **1**, Coon et al. have shown that some of the mutant enzymes perform more olefin epoxidation at the expense of C−H hydroxylation with substrates, such as 2-butene, cyclohexene, etc., that have the two options.[11] Their proposed multioxidant hypothesis is shown in Scheme 1a, which specifies the roles assigned to the three key species **1**−**3**.

A further challenge to the "single-oxidant hypothesis" was mounted by the studies of Newcomb et al., which were summarized recently in an *Accounts of Chemical Research* article.[16] Thus, they used a series of clock substrates, shown in Scheme 1b, which can distinguish whether the substrates undergoing monooxygenation are converted to a radical intermediate or to a "cationic" intermediate, by the mode of rearrangement. These substrates were subjected[16] to P450 monooxygenation using the wild type and mutant (T → A) enzymes of Coon et al.[11] The observation of a large amount of cationic derived products that increased for the mutants led Newcomb to hypothesize that alongside Cpd I (**1**), there is a second oxidant that inserts OH^+ and generates a protonated alcohol product, which subsequently rearranges in a manner typical to carbocations. Newcomb et al. proposed that the source of the protonated alcohol is the iron(III)-hydroperoxo species, **2**, that inserts OH^+ into the C−H bond in addition to its epoxidation capability (Scheme 1b). Furthermore, for the enzyme chloro peroxidase (CPO), the iron(III)-hydroperoxo, **2**, is not formed in the cycle, and, in accord, the probe substrate (1-phenyl-2-methylcyclopropane) does not undergo any phenyl hydroxylation,[17] which is a proposed marker reaction of **2**. The possible participation of **2** in oxidative processes is further corroborated by findings that in the enzyme heme-oxygenase (HO-1), a species such as **2** (but with a histidine proximal ligand) is responsible for the self-hydroxylation of the meso carbon position of the heme, leading eventually to heme catabolism.[18−23] Pratt et al.[22] and

(9) Egawa, T.; Shimada, H.; Ishimura, Y. *Biochem. Biophys. Commun.* **1994**, *201*, 1464−1469.
(10) Schlichting, I.; Berendzen, J.; Chu, K.; Stock, A. M.; Maves, S. A.; Benson, D. E.; Sweet, R. M.; Ringe, D.; Petsko, G. A.; Sligar, S. G. *Science* **2000**, *287*, 1615−1622.
(11) Vaz, A. D. N.; McGinnity, D. F.; Coon, M. J. *Proc. Natl. Acad. Sci. U.S.A.* **1998**, *95*, 3555−3560.
(12) Vaz, A. D. N.; Roberts, E. S.; Coon, M. J. *J. Am. Chem. Soc.* **1991**, *113*, 5886−5887.
(13) Roberts, E. S.; Vaz, A. D. N.; Coon, M. J. *Proc. Natl. Acad. Sci. U.S.A.* **1991**, *88*, 8963−8966.
(14) Vaz, A. D. N.; Kessell, K. J.; Coon, M. J. *Biochemistry* **1994**, *33*, 13651−13661.
(15) Vaz, A. D. N.; Pernecky, S. J.; Raner, G. M.; Coon, M. J. *Proc. Natl. Acad. Sci. U.S.A.* **1996**, *93*, 4644−4648.
(16) Newcomb, M.; Toy, P. H. *Acc. Chem. Res.* **2000**, *33*, 449−455.
(17) Toy, P. H.; Newcomb, M.; Hager, L. P. *Chem. Res. Toxicol.* **1998**, *11*, 816−823.
(18) Fujii, H.; Zhang, X.; Tomita, T.; Ikeda-Saito, M.; Yoshida, T. *J. Am. Chem. Soc.* **2001**, *123*, 6475−6484.
(19) Auclair, K.; Moënne-Loccoz, P.; Ortiz de Montellano, P. R. *J. Am. Chem. Soc.* **2001**, *123*, 4877−4885.
(20) Yoshida, T.; Migita, C. T. *J. Inorg. Biochem.* **2000**, *82*, 33−41.

Scheme 2. Potential "Second Oxidant" Species

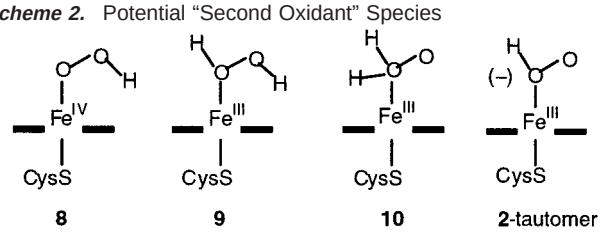

Peisach et al.[24] further argue in favor of a species such as **2** as the sole oxidant in P450 and related monooxygenations.

More indirect evidence for the presence of a second oxidant keeps accumulating from mechanistic studies of mimetic systems. However, there seems to be a variety of reasonable alternative formulations of the second oxidant. Thus, Nam et al.[25−28] provided evidence that an iron(III)-OOR (R = H, alkyl, acyl) species can epoxidize olefins prior to its heterolytic cleavage to Cpd I type species. The studies show that the process critically depends on the presence and identity of a sixth ligand coordination to the iron(III) center.[26,27] However, some of the formulations of the oxidant by Nam et al. correspond to an iron-(IV)-OOR (e.g. **8**, Scheme 2) rather than to the iron(III) species. Collman et al.[29] demonstrated that the branching ratio of the products for iron(III)porphyrin catalysts depends on the identity of the oxygen donor (XO = PhIO, F_5PhIO, etc.), thereby implying the existence of a second oxidant formulated as iron-(III)-OX, alongside Cpd I. Another formulation of the second oxidant is the hydrogen peroxide complex, iron(III)-H_2O_2 (e.g. **9**, Scheme 2). Such a species has been considered, for example, by Newcomb,[16] as an alternative to **2**, and was favored by Pratt.[22] There are pro and con arguments to consider **9** as a "second oxidant". In the P450 cycle, it is thought that **9** nascent from **2** by protonation of the proximal oxygen is responsible for the oxygen wasting "uncoupling" reaction.[30] Furthermore, the iron(III)-hydrogen peroxide complex incurs in the catalytic cycles of peroxidase enzymes CPO,[4] and in its laboratory made mimics,[31] but its participation in monooxygenation processes has not been suggested for either species. For CPO itself the monooxygenation activity is ascribed to its well-known Cpd I (**1**) species. In fact, the results of Newcomb et al.[17] that CPO does not perform phenyl epoxidation of their probe substrate imply that **9** is not the sought for oxidant. Despite these arguments, **9** could still be a potent oxidant. Thus, in some mechanistic schemes,[23] the self-hydroxylation of the iron(III)-OOH species of the enzyme HO-1 is described to transpire with protonation at the proximal oxygen of **2**. While the mechanism of the protonation has not been specified,[23] the protonation may already exist in terms of the iron(III)-H_2O_2 complex, **9**. Another candidate species that certainly seems to be prepared for oxygen transfer is the tautomer of **2** (Scheme 2). Finally, Hata et al.[32] have proposed that the diprotonated species **10** is an oxidant far superior to Cpd I. Clearly, the question of a second oxidant is inherently complex.

The mounting evidence of the presence of more than one oxidant in the catalytic cycle of P450 is a call for theory to complement experiment and decipher by means of electronic structure calculations the identity of such oxidants and their monooxygenation mechanisms with alkanes and alkenes. In view of the number of alternative oxidants, augmented by the possibility of multiple mechanisms of monooxygenation for each oxidant, the entire task is formidable even for theory. A stepwise screening of the various possibilities is our strategy that begins with the present paper. The recent assignment of **2** by ENDOR/EPR spectroscopies[3] and its strong implication as a second electrophilic species capable primarily of epoxidizing alkenes (Scheme 1)[11−16] make it the ideal first candidate. The present paper is therefore devoted to the electronic structure and potential reactivity of iron(III)-hydroperoxo as an epoxidizing agent.

II. Target Species and Goals

The study was carried out with density functional theory. The technical details, similar in most of our past computational studies in the P450 field,[33−43] are described in the Theoretical Methods section. The aspects addressed in the present study, which rely on a model system having a pristine porphine and an HS^- as a proximal ligand, are outlined in Scheme 3. These simplifications were made in previous studies, which showed that the species are reasonable models for the more complex system.[34−37] Some of these species were studied before by Harris and Loew[30,44,45] using mercaptide as a ligand and a different level of theory than the one used here (see Theoretical Methods section). A comparison with their results would be a very useful benchmark for the reliability of both sets of conclusions.

The first issue in Scheme 3(i) concerns the electronic structure of **2** and its tautomer, indicated in Scheme 3 as **2d** and **2p** where **d** refers to the distal site of protonation, and **p** refers to the proximal. The species **2p** was considered already by Harris and Loew[30,44,45] and was ruled out as a potential bifurcation species

(21) Messinger, J.; Robblee, J. H.; Bergmann, U.; Fernandez, C.; Glatzel, P.; Visser, H.; Cinco, R. M.; McFarlane, K. L.; Bellacchio, E.; Pizarro, S. A.; Cramer, S. P.; Sauer, K.; Klein, M. P.; Yachandra, V. K. *J. Am. Chem. Soc.* **2001**, *123*, 7804−7820.
(22) Pratt, J. M.; Ridd, T. I.; King, L. J. *J. Chem. Soc., Chem. Commun.* **1995**, 2297−2298.
(23) Ortiz de Montellano, P. R. *Acc. Chem. Res.* **1998**, *31*, 543−549.
(24) Sam, J. W.; Tang, X.-J.; Peisach, J. *J. Am. Chem. Soc.* **1994**, *116*, 5250−5256.
(25) Lee, K. A.; Nam, W. *J. Am. Chem. Soc.* **1997**, *119*, 1916−1922.
(26) Nam, W.; Lim, M. H.; Oh, S.-Y.; Lee, J. H.; Lee, H. J.; Woo, S. K.; Kim, C.; Shin. W. *Angew. Chem.* **2000**, *39*, 3646−3649.
(27) Nam, W.; Lim, M. H.; Moon, S. K.; Kim, C. *J. Am. Chem. Soc.* **2000**, *122*, 10805−10809.
(28) Nam, W.; Lee, H. J.; Oh, S.-Y.; Kim, C.; Jang, H. G. *J. Inorg. Biochem.* **2000**, *80*, 219−225.
(29) Collman, J. P.; Chien, A. S.; Eberspacher, T. A.; Brauman, J. I. *J. Am. Chem. Soc.* **2000**, *122*, 11098−11100.
(30) Harris, D. L.; Loew, G. H. *J. Am. Chem. Soc.* **1998**, *120*, 8941−8948.
(31) Woggon, W. D.; Wagenknecht, H. A.; Claude, C. *J. Inorg. Biochem.* **2001**, *83*, 289−300.
(32) Hata, M.; Hoshino, T.; Tsuda, M. *Chem. Commun.* **2000**, 2037−2038.
(33) Filatov, M.; Harris, N.; Shaik, S. *J. Chem. Soc., Perkin Trans. 2* **1999**, 399−410.
(34) Ogliaro, F.; Cohen, S.; Filatov, M.; Harris, N.; Shaik, S. *Angew. Chem., Int. Ed.* **2000**, *39*, 3851−3855.
(35) Ogliaro, F.; Cohen, S.; de Visser, S. P.; Shaik, S. *J. Am. Chem. Soc.* **2000**, *122*, 12892−12893.
(36) Ogliaro, F.; de Visser, S. P.; Cohen, S.; Kaneti, J.; Shaik, S. *ChemBioChem* **2001**, *3*, 848−851.
(37) Ogliaro, F.; de Visser, S. P.; Groves, J. T.; Shaik, S. *Angew. Chem., Int. Ed.* **2001**, *40*, 2874−2878; erratum p 3503.
(38) de Visser, S. P.; Ogliaro, F.; Gross, Z.; Shaik, S. *Chem.-Eur. J.* **2001**, *7*, 4954−4960.
(39) Harris, N.; Cohen, S.; Filatov, M.; Ogliaro, F.; Shaik, S. *Angew. Chem., Int. Ed.* **2000**, *39*, 2003−2007.
(40) Ogliaro, F.; Harris, N.; Cohen, S.; Filatov, M.; de Visser, S. P.; Shaik, S. *J. Am. Chem. Soc.* **2000**, *122*, 8977−8989.
(41) de Visser, S. P.; Ogliaro, F.; Harris, N.; Shaik, S. *J. Am. Chem. Soc.* **2001**, *123*, 3037−3047.
(42) de Visser, S. P.; Ogliaro, F.; Shaik, S. *Angew. Chem., Int. Ed.* **2001**, *40*, 2871−2874.
(43) de Visser, S. P.; Ogliaro, F.; Shaik, S. *Chem. Commun.* **2001**, 2322−2323.
(44) Harris, D. L.; Loew, G. H.; Waskell, L. *J. Am. Chem. Soc.* **1998**, *120*, 4308−4318.
(45) Loew, G. H.; Harris, D. L. *Chem. Rev.* **2000**, *100*, 407−419.

Scheme 3. Model Systems and Target Issues of the Theoretical Study

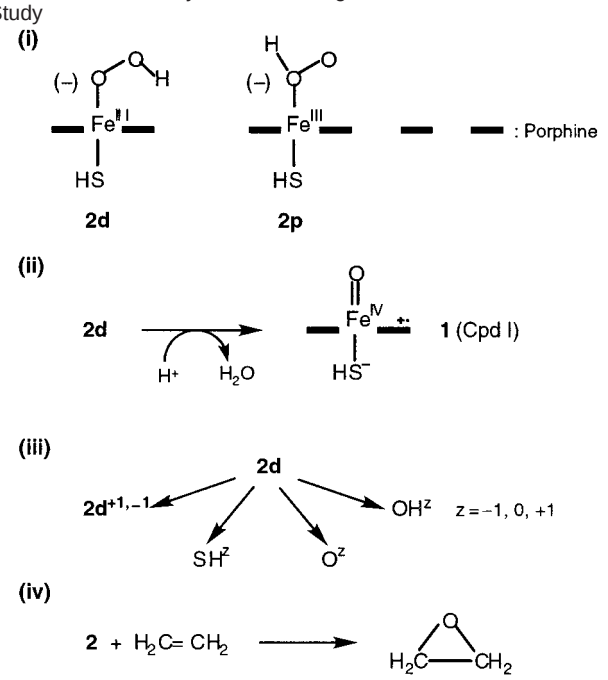

leading to the "uncoupling" reaction. Here we address also its potential as a monooxygenating species viz. **2d**. We study the ground states of these species as isolated molecules and under the influence of a polarizing medium, as well as their low energy excited states that can potentially be involved in monooxygenation, as found for Cpd I.[40,41] A second important aspect (ii) of the iron(III)-OOH species **2d** is its alleged capacity to generate Cpd I by water release as a result of distal oxygen protonation. The precise machinery behind the proton delivery starts to be understood, and the proton source is now believed to be a bulk water molecule sequestered[3,46] in the pocket of the enzyme. Here we compare the protonation by a bare proton, by H_3O^+, and by a water molecule. A study of issues (i) and (ii) will also afford an opportunity to test the viability of our model systems against the more complex species described in the pioneering theoretical study of Harris and Loew.[30]

The third issue (iii) is related to the propensity of the target species, **2d**, to lose OH^z, O^z, and HS^z species ($z = 0, +1, -1$). This issue probes, on one hand, the Fe−O, O−O, and Fe−S bond strengths of the putative oxidant (**2**) and, on the other hand, addresses the monooxygenation capability of the species, as well as the putative role of the thiolate ligand to facilitate the O−O bond cleavage en route to the formation of Cpd I.[1,4−8] In addition, the electron attachment and ionization energies of **2** are studied and also compared with those of some relevant oxidant species.

The species, $[PorSHFeOOH]^{-1,0,-2}$ ($\mathbf{2d}^{0,+1,-1}$), [PorSHFeOOH]$^{-1}$ (**2p**), [PorSHFeO] (Cpd I, **1**), $[PorSHFeO]^{-1}$ (Cpd II, $\mathbf{11} = \mathbf{1}^{-1}$), $[PorSHFeO]^{-2}$ (Cpd III, $\mathbf{1}^{-2}$), $[PorSHFeOH]^{0,-1,-2}$ (**12**), $[PorFeO]^{1,0,-1}$ (**13**), $[PorFeOOH]^{+1,0,-1}$ (**14**), [PorSHFeOH$_2$], etc., necessary to the study of our first three issues (i), (ii), and (iii) were fully optimized and characterized for several spin states and configurations. Altogether the study involved about 50 species.[47] These data are collected in Tables S1−S5 of the Supporting Information.

(46) Vidakovic, M.; Sligar, S. G.; Li, H.; Poulos, T. L. *Biochemistry* **1998**, *26*, 9211−9219.

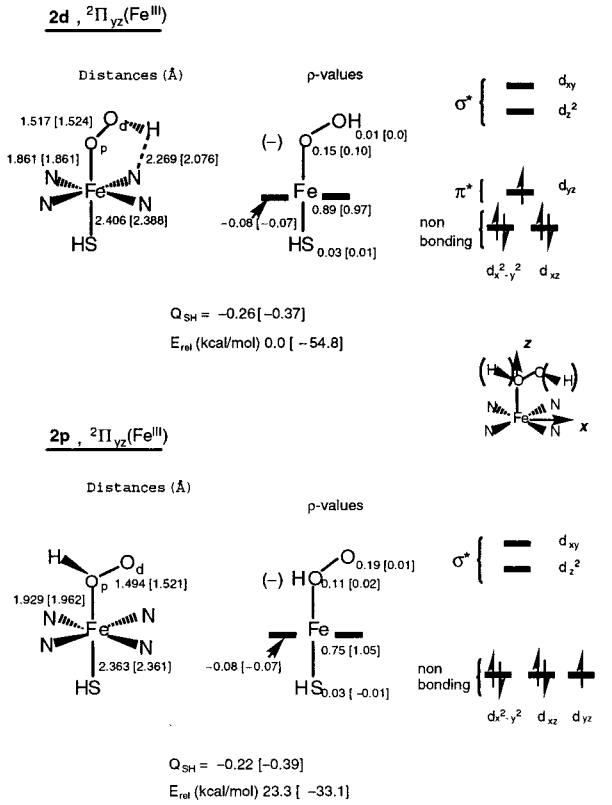

Figure 2. Geometric parameters (Å and deg), relative energies (kcal/mol), group spin densities (ρ), group charges (Q), and electronic structures of **2d** and **2p**. Values in square brackets refer to the species in a polarizing medium ($\epsilon = 5.7$), while values out of brackets refer to the isolated species. The electron occupancy in the d-block is shown near each species.

Finally, the last issue in Scheme 3 (iv) concerns the epoxidation capability of **2** toward ethene as a model alkene, which is considered as marker process of **2** as an oxidant. The possible pathways involve transfer of the distal and/or proximal oxygens. All the processes will be studied along concerted and stepwise pathways. Comparison with the corresponding processes of Cpd I[41] will enable us to answer the question: Is iron(III)-OOH by itself a viable oxidant?

III. Results and Discussion

A. Electronic Structure of 2d and 2p in Vacuum and with Medium Polarization. The hydroperoxo complex is believed to be generated by the protonation of the reduced oxyferrous $[FeOO]^{-2}$ complex.[1,3] A priori, H^+ can be added either on the proximal oxygen (O_p) or on the distal oxygen (O_d) leading to **2d** and **2p**, respectively. The key features and relative energies of these species are displayed in Figure 2, alongside simplified diagrams of the d-block orbitals. The Fe−S and O−O distances

(47) For a sample of other theoretical studies of Cpd I of P450, see for example; (a) Green, M. T. *J. Am. Chem. Soc.* **1999**, *121*, 7939−7940. (b) Green, M. T. *J. Am. Chem. Soc.* **2000**, *122*, 9495−9499. (c) Harris, D. L.; Loew, G. H. *J Porphyrins Phthalocyanines* **2001**, *5*, 334−344. (d) Harris, D. L.; Loew, G. H.; Waskell, L. *J. Inorg. Biochem.* **2001**, *83*, 309−318. (e) Anthony, J.; Grodzicki, M.; Trautwein, A. X. *J. Phys. Chem. A* **1997**, *101*, 2692−2701. (f) Ohta, T.; Matsuura, K.; Yoshizawa, K.; Morrishima, J. *J. Inorg. Biochem.* **2000**, *82*, 141−152. (g) Yoshizawa, K.; Kagawa, Y.; Shiota, Y. *J. Phys. Chem. B* **2000**, *104*, 12365−12370. (h) For calculations of Cpd II with an imidazole proximal ligand see: Kuramochi, H.; Noodleman, L.; Case, D. A. *J. Am. Chem. Soc.* **1997**, *119*, 11442−11451. Deeth, R. J. *J. Am. Chem. Soc.* **1999**, *121*, 6074−6075. (i) For pentacoordinated Cpd I and Cpd II species see: Ghosh, A.; Almlöf, J.; Que, L., Jr. *J. Phys. Chem.* **1994**, *98*, 5576−5579.

Table 1. Electronic Structure, Relative Energies, Key Geometric[a] Features, and Group Spin Densities of the Tautomers **2p** and **2d** of $[Por(SH)FeOOH]^{-1}$

				distances (Å)						group spin densities				
tautomer	states	configuration	*E* (kcal/mol)	Fe–S	Fe–O	O–O	Fe–N	Δ^b	H–N	Fe	O	OH	SH	Por
2d	$^2\Pi_{yz}(Fe^{III})$	$a_{2u}^2d_{x2-y2}^2d_{xz}^2\pi^*_{yz}{}^1$	0.0	2.406	1.861	1.517	2.025	+0.009	2.269	0.895	0.151	0.011	0.026	−0.077
2d.sol[c]	$^2\Pi_{yz}(Fe^{III})$	$a_{2u}^2d_{x2-y2}^2d_{xz}^2\pi^*_{yz}{}^1$	−54.81	2.388	1.861	1.524	2.025	+0.023	2.076	0.966	0.103	−0.002	0.0	−0.067
2d	$^2\Delta_{xz}(Fe^{III})$	$a_{2u}^2d_{x2-y2}^2d_{xz}^1\pi^*_{yz}{}^2$	+11.09	2.465	1.965	1.520	2.021	+0.012	2.286	1.144	−0.065	0.016	−0.046	−0.049
2d[d]	$^2\Delta_{x^2-y^2}(Fe^{III})$	$a_{2u}^2d_{x2-y2}^1d_{xz}^2\pi^*_{yz}{}^2$	+17.22	2.471	1.957	1.551	2.021	+0.031	2.411	1.241	−0.088	−0.005	−0.069	−0.079
2d	$^2A_{2u}(Fe^{II})$	$a_{2u}^1d_{x2-y2}^2d_{xz}^2\pi^*_{yz}{}^2$	+36.66	2.565	2.002	1.539	2.016	+0.036	2.541	0.053	0.112	0.012	0.356	0.467
2d	$^4A(Fe^{III})$	$a_{2u}^2d_{x2-y2}^2d_{xz}^1\pi^*_{yz}{}^1\sigma^*_{z2}{}^1$	+16.75[e]	2.692	2.028	1.506	2.029	+0.037	2.471	2.475	0.355	0.054	0.227	−0.111
2d	$^6A(Fe^{III})$	$a_{2u}^2d_{x2-y2}^1d_{xz}^1\pi^*_{yz}{}^1\sigma^*_{z2}{}^1\sigma^*_{xy}{}^1$	+14.89[e]	2.601	2.013	1.496	2.090	−0.339	2.357	3.970	0.382	0.055	0.254	0.339
2d	$^6E_g(Fe^{III})$	$a_{2u}^1d_{x2-y2}^1d_{xz}^1\pi^*_{yz}{}^2\sigma^*_{z2}1e_g(Por)^1$	+46.98	2.422	1.864	1.509	2.096	+0.047	2.247	2.925	0.010	−0.021	−0.014	2.100
				Fe−S	Fe−O	O−O	Fe−N	Δ^b		Fe	OH	O	SH	Por
2p	$^2\Pi_{yz}(Fe^{III})$	$a_{2u}^2d_{x2-y2}^2d_{xz}^2d_{yz}^1$	+23.32	2.363	1.929	1.494	2.021	−0.046		0.759	0.106	0.190	0.029	−0.084
2p.sol[c]	$^2\Pi_{yz}(Fe^{III})$	$a_{2u}^2d_{x2-y2}^2d_{xz}^2d_{yz}^1$	−33.12	2.361	1.962	1.521	2.020	−0.021		1.054	0.015	0.010	−0.007	−0.072
2p	$^2\Pi_{xz}(Fe^{III})$	$a_{2u}^2d_{x2-y2}^2d_{xz}^1d_{yz}^2$	+26.24	2.363	2.014	1.525	2.021	−0.065		0.948	−0.007	0.064	0.049	−0.054
2p[f]	$^2\Delta_{x}{}^2{}_{-y}{}^2(Fe^{III})$	$a_{2u}^2d_{x2-y2}^1d_{xz}^2d_{yz}^2$	+35.38							1.026	−0.006	0.039	−0.012	−0.047
2p	$^4A(Fe^{III})$	$a_{2u}^2d_{x2-y2}^2d_{xz}^1d_{yz}^1\sigma^*_{z2}{}^1$	+31.16	2.632	2.226	1.466	2.026	−0.066		2.327	0.148	0.411	0.248	−0.234
2p	$^6A(Fe^{III})$	$a_{2u}^2d_{x2-y2}^1d_{xz}^1d_{yz}^1\sigma^*_{z2}{}^1\sigma^*_{xy}{}^1$	+28.73	2.548	2.247	1.447	2.071	−0.209		3.885	0.164	0.478	0.238	0.235

[a] Except where stated, all structures are optimized without symmetry constraint at the UB3LYP/LACVP+ECP level of theory. Additional geometric details are provided in the Supporting Information (Table S1). [b] Δ is the distance between Fe and the porphine average plane (Δ > O means FeO above the average plane; Δ < O means FeO below the average plane). [c] Full optimization with solvent effect ($\epsilon = 5.7$). [d] Optimization carried out within the C_s symmetry group. [e] With LACV3P+*(6-311+G*) these data are 14.52 and 11.23 kcal/mol, respectively. [f] Single point calculation on the **2p** $^2\Pi_{xz}(Fe^{III})$ geometry.

are slightly longer than those reported for these species by Harris and Loew,[30] as might be expected from the different functionals and basis sets used in the two studies. Otherwise, the two sets of results are very similar, and so are the relative energies that favor **2d** by 23.3 (21.7 with medium polarization effect) kcal/mol here and 18.4 kcal/mol in Harris and Loew.[30]

The electronic structures of the two species are very similar, both being monoradicals designated as $^2\Pi_{yz}(Fe^{III})$. This term symbol specifies the location of the single electron in an antibonding orbital made from the d_{yz} type orbital on the iron and the p_y orbital of the proximal oxygen. The spin densities, in Figure 2, indeed show that an unpaired electron is mostly located on the iron, and medium polarization further increases this character. The orbital diagram shows that the main difference between the two tautomers is in the level of the d_{xz} and d_{yz} orbitals. In **2d** the d_{yz} orbital is higher lying because it is an antibonding $\pi^*(FeO_p)$ orbital made from a mixture of the $Fe(d_{yz})$ and $O_p(p_y)$ atomic orbitals. In contrast, in **2p** the d_{yz} and d_{xz} orbitals are almost degenerate since the $O_d(p_x)$ orbital of the protonated site is less available to mix with the $Fe(d_{yz})$ orbital. Indeed, **2p** has another low lying state, with a $^2\Pi_{xz}(Fe^{III})$ configuration, and this state lies only 2.92 kcal/mol above the ground state (see Table 1 above).

The relative stability of these two isomers of **2** is rationalizable by consideration of the bonding between the Fe^{III} center and the OOH moiety, and the interaction of the latter moiety with the porphine. In **2d** the p_y orbital of the proximal oxygen (O_p) can interact with the d_{yz} orbital of iron to form a π(FeO) bond, whereas in **2p** the p_x orbital is engaged primarily in the O_p-O_d and O_p-H bonding and is less available for interaction with the iron. As such, the Fe−O interaction is stronger in **2d**, and the corresponding bond is indeed shorter. In addition, **2d** maintains an $O_dH\cdots N_{por}$ hydrogen bond with the nitrogen atom of the porphine. The two effects contribute to the superior stability of **2d**, which remains the more stable tautomer also with inclusion of medium polarization (see Figure 2). Because the energy difference between the two species is ca. 20 kcal/mol, while the barrier for ethene epoxidation by Cpd I calculated by us recently is ca. 14 kcal/mol,[41] **2p** cannot be considered a candidate for a "second oxidant", and we are left with **2d** as the optional oxidant.[48a]

To verify that the $^2\Pi_{yz}(Fe^{III})$ state of **2d** is well separated from its excited states, we fully optimized a series of low-lying excited states of **2d**. These results are collected in Table 1 using term symbols that derive from the orbital occupancy in the d-block diagram shown in Figure 2. Other states of **2d**, including an extended set of low-lying states of **2p**, are also collected in Table 1. The results confirm that there is no ambiguity regarding the nature of the ground state of the iron(III)-hydroperoxo complex, **2d**. The $^2\Pi_{yz}$ ground state is well separated from other states by more than 11 kcal/mol. The key finding here is that, in contrast to Cpd I that has a virtually degenerate ground state and exhibits a two-state-reactivity,[40,41] iron(III)-hydroperoxo will most likely feature a single state reactivity (SSR).[48b] Hereafter, we focus on the properties of **2d** and its monooxygenation capabilities nascent from the ground state, $^2\Pi_{yz}(Fe^{III})$.

B. Iron(III)-OOH, 2d − Its Geometry and Bonding Properties as Compared with Cpd I. As mentioned before, an interesting structural feature of **2d**, in Figure 2, is the internal $O_dH\cdots N_{Por}$ hydrogen bonding. Medium polarization does not change this feature, but, on the contrary, this hydrogen bond is further strengthened, since the partial negative charge of the nitrogen atoms in the porphyrin as well as the electropositive character of the hydrogen atom both increase by the polarizing medium. This, however, does not mean that the same structure will be assumed also in the protein pocket, where it could well be replaced by an external hydrogen bond. The polarization also

(48) (a) There will be a barrier for the **2d** → **2p** rearrangement. This barrier, in addition to the ∼20 kcal/mol endothermicity of **2p**, will make the total barrier for epoxidation by **2p** higher than 20 kcal/mol, which is already much higher than the barrier for epoxidation by Cpd I.[41] (b) For a similar reason, we do not investigate the reactions of the excited states of **2d**, which would be relevant only if leading to barrierless processes.

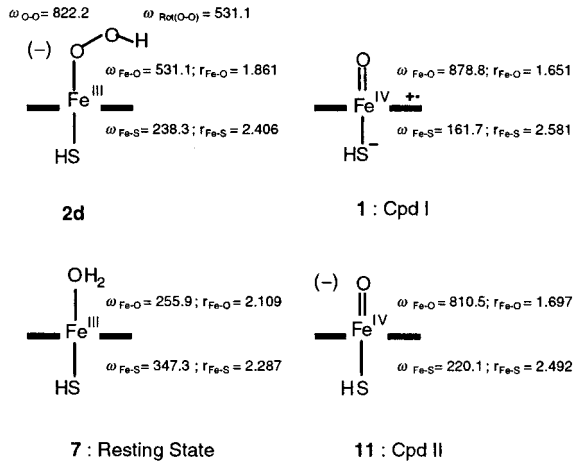

Figure 3. (a) A few key frequencies (cm^{-1}) and bond distances (Å) of **2d** as compared to other species.

shortens the Fe−S bond from 2.406 to 2.388 Å, and as already explained elsewhere,[34−36] this is attended by an increase of the thiolate ($S:^-$) character (Q_{SH} initially at −0.267 becomes −0.369 with polarization effect). Indeed, the Fe−S bond seems here to be again the most flexible among the bonds of the complex, as found computationally for Cpd I,[34−36] and as deduced experimentally for the resting state by various probes including mutation studies.[4,49,50]

Figure 3 shows a few key frequencies of **2d** as compared with Cpd I (**1**), Cpd II (**11**), and the resting state (**7**). Interestingly, the rotation about the O−O bond in **2d** is very soft, and an external bond in the protein pocket can easily replace the internal hydrogen bond (OH- - -N_{por}). The frequency of the Fe−S bond is the smallest for Cpd I[47f] that has the longest Fe−S bond (2.581 Å), largest for the low-spin resting state with the shortest Fe−S bond (2.288 Å), and intermediate for **2d** with the intermediate bond length (2.406 Å).

Fe−S Bonding. The nature of the Fe−S bond of **2d** can be further appreciated by looking at the computed energies in Figure 4. The Fe−S bond energy of **2d** is seen to be appreciable, 34.0 kcal/mol, as compared with the meager 7.95 kcal/mol in Cpd I.[51] Another major difference with Cpd I is the dissociation limit. Thus, while in Cpd I the Fe−S bond breaks into a thiolyl radical and a neutral $PorFe^{IV}O$ species,[34] in **2d** the bond breaks into thiolate anion and a neutral $PorFe^{III}OOH$. This major difference is a result of the unique electronic structure of Cpd I that possesses an unpaired electron in an "a_{2u}" type orbital made from the porphyrin pure a_{2u} and the σ-hybrid of the thiolate ligand.[34−36] Because this is a singly occupied orbital, the resulting Fe^{IV}−S bond is a resonance hybrid of two forms, one (**a**) having a normal two-electron bond in a cation radical porphyrin complex and the other (**b**) having a one-electron bond in a porphyrin saturated complex (see Figure 4b). This blend makes the Fe^{IV}−S bond rather weak,[34] very flexible (ω_{Fe-S} = 161.7 cm^{-1}), and the species as a whole exhibits a chameleon behavior.[35−37] In contrast, as shown in Figure 4b, the Fe^{III}−S bond of **2d** is primarily made of the strong two-electron bond type in a formally saturated porphyrin complex. This last feature

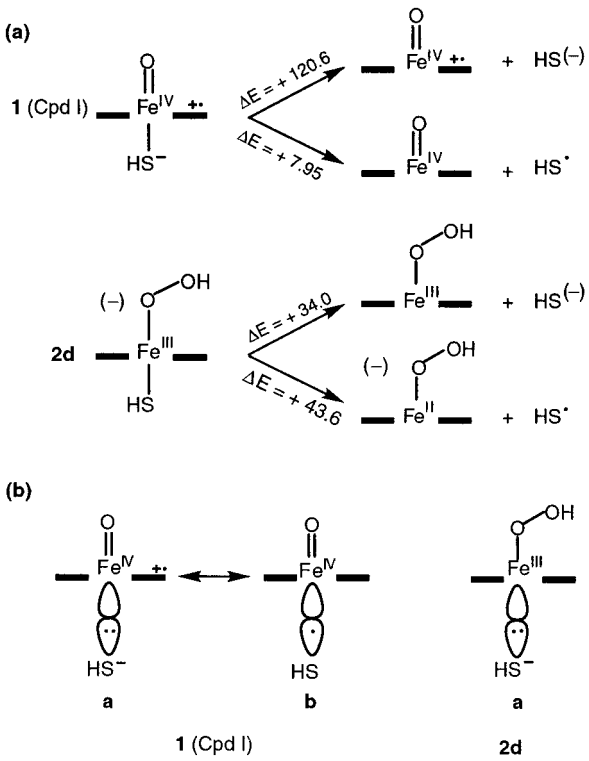

Figure 4. (a) Fe−S bond dissociation energies (kcal/mol) of **2d** as compared with those in Cpd I. (b) Description of the Fe−S bond using leading resonance structures (for brevity, the two-electron bond is described with the structure that keeps two electrons on the ligand in line with the oxidation state formalism).

prohibits any sulfur → porphyrin spin transfer and consequently confers a very little chameleon aptitude to **2d**.

Fe−O versus O−O Bonding. Figure 5 shows data for gauging the O−O versus Fe−O bond strengths of **2d**. The right-hand side of the figure shows various modes of O−O bond cleavage. The O−O bond energy is seen to be significant, 31.7 kcal/mol, albeit smaller than the corresponding bond in hydrogen peroxide ($D_{O-O}(H_2O_2)$ = 46.4 kcal/mol at the same level). The left-hand side of Figure 5 shows the energy involved in a loss of the proximal oxygen species. From these data it is clear that **2d** as such will not participate in transfer of OH^+, and its most probable reactive capability would be the transfer of neutral OH or O species.

Electron Acceptor Properties. Other properties, which are associated with a potential reactivity pattern, are the electron attachment and ionization energies of the species. Figure 6 shows the energy relationship of **2d** to its monooxidized and monoreduced forms with and without a thiolate ligand. These data are compared with the corresponding data for Cpd I, its reduced form, Cpd II, and the direduced form which we refer to here as Cpd III. It is seen that both Cpd II and **2d** hold on well to their extra electron (ionization energies > 60 kcal/mol). However, both are poor electron acceptors. Their dianionic species are computed to be unstable and will lose one electron spontaneously. The data on the right-hand side highlight the internal donor ability of the thiolate.[2,4−8] Thus, in the absence of thiolate ligation, much higher energy is required to remove an electron from either the Fe^{III} species (**14**) or Cpd II (**13**). This effect is associated with the destabilization of the a_{2u} orbital by thiolate ligation.[7,33,52]

(49) Roach, M. P.; Pond, A. E.; Thomas, M. R.; Boxer, S. G.; Dawson, J. H. *J. Am. Chem. Soc.* **1999**, *121*, 12088−12093.
(50) Sigman, J. A.; Pond, A. E.; Dawson, J. H.; Lu, Y. *Biochemistry* **1999**, *38*, 11122−11129.
(51) The datum of 6.9 kcal/mol in ref 34 refers to Cpd I in C_s symmetry.

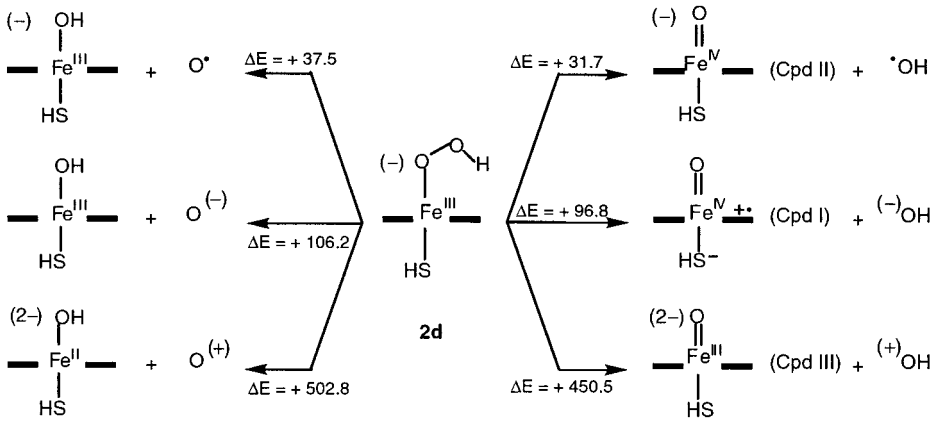

Figure 5. Fe−O and bond dissociation energies and O^z extrusion energies (kcal/mol) for **2d**.

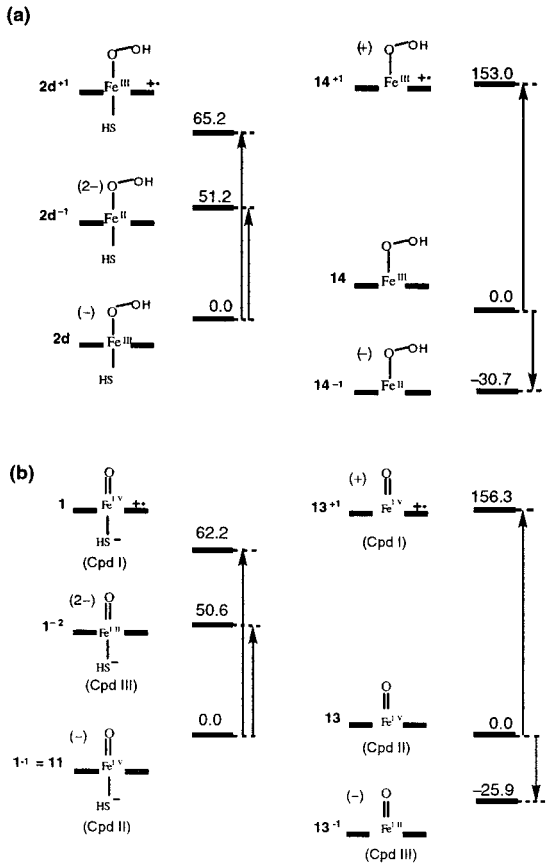

Figure 6. Relative energies (kcal/mol) of the singly reduced and singly oxidized forms of (a) **2d** and (b) Cpd II. On the right-hand side we show the same energetics for the species devoid of the thiolate ligand.

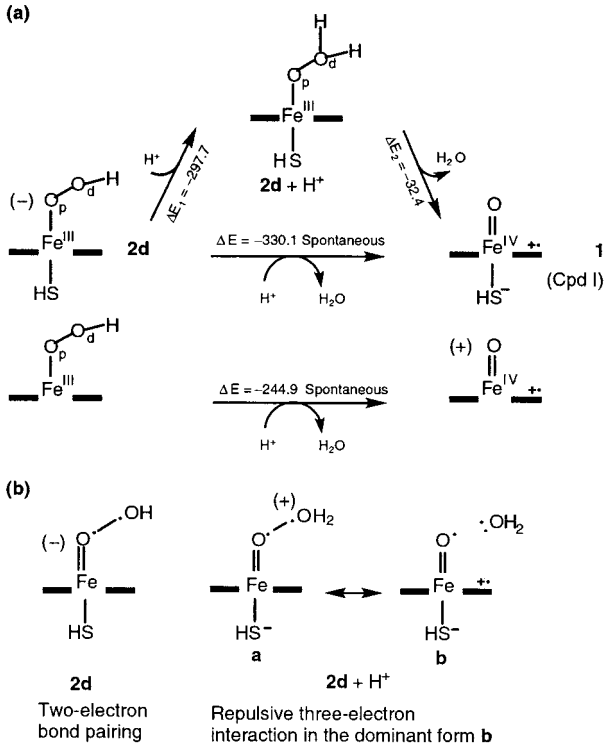

Figure 7. (a) Protonation energies (kcal/mol) of **2d** at the distal oxygen. The process involves simultaneous expulsion of H_2O to form Cpd I. A constrained stepwise process is shown where initially Fe−O_p and O_p−O_d are kept constant to give **2d** + $\mathbf{H}^+$, followed by water release. Underneath we show the same process without a thiolate ligand. The proton affinities are given by the ΔE values near the arrows. (b) Description of the electron pairing in the O−O bond in **2d** viz. in the protonated form (**2d** + $\mathbf{H}^+$) using leading resonance structures (the unpaired electron on the oxygen in Cpd II is one of the electrons in the $\pi^*(d_{xz})$ or $\pi^*(d_{yz})$ orbitals of the FeO moiety).

Behavior of 2d Under Protonation. In agreement with the previous study of Harris and Loew,[30] our calculations, summarized in Figure 7a, show that the addition of a proton to the oxygen distal position leads to a barrier-free formation of Cpd I by water release. To understand the instability of **2d** toward distal protonation, we carried out the calculations in two consecutive steps (Figure 7a). In the initial step, the H^+ is added to **2d**, and the "intermediate" species is fully optimized with exception of the Fe−O_p and O_p−O_d bonds that are kept frozen at their value in **2d**. In the second step, the water molecule is allowed to detach and thereby lead to Cpd I. The first step is almost alone responsible for the large proton affinity, while the contribution of the second step is marginal.

The computed overlap population of the O_p−O_d bond reveals that upon protonation, it decreases from a positive value (+0.062) to a negative one (−0.055). This just highlights the fact that the O_p−O_d bond is broken as soon as the proton is added, but it does not explain the origins of this bond weakening. Using the constituent resonance structures of the O−O bond, before and after protonation, leads to a simple explanation. Thus, the O−O bond can be understood to result from the interaction

(52) Hanson, L. K.; Chang, C. K.; Davis, M. S.; Fajer, J. *J. Am. Chem. Soc.* **1981**, *103*, 663−670.

of either OH or H_2O species with a Cpd II type species, as shown in Figure 7b. Cpd II has unpaired electrons in its FeO moiety (in the π^*(FeO) orbitals[33]). In **2d** the unpaired electrons of the OH• and Cpd II moieties can couple to create a normal two-electron bond. However, in the protonated form (**2d** + H^+), such pairing of two unpaired electrons can transpire only through the involvement of a high-energy resonance structure (**a**) in which the H_2O moiety appears as a radical cation. Consideration of the ionization energy of H_2O viz. the electron attachment energy of Cpd I (Figure 6) shows immediately that this resonance structure **a** lies well above structure **b** that involves neutral H_2O and a Cpd I species. In form **b**, the O−O interaction involves three electrons and is therefore repulsive, rendering this bond simultaneously dissociative, as revealed by the negative overlap population of the frozen O−O bond of the protonated form.

The computed proton affinity of **2d** in Figure 7a is significant (−330.1 vs −334 kcal/mol in Harris and Loew[30]) and indicates that **2d** is a fairly strong base. According to recent experimental results, the proton source is possibly a hydronium (H_3O^+) ion held by a hydrogen bonding network.[46] Using H_3O^+ as the proton source, the process of Cpd I production is still very exothermic (−146.5 kcal/mol), while the use of H_2O results in an endothermic process (+96.0 kcal/mol). Thus, the basicity of **2d** is between those of water and OH^-. It is important to recognize that the anionic moiety of Asp251 that holds H_3O^+ also accentuates its proton affinity. A simple electrostatic calculation of this interaction shows that such a negative charge placed ca. 2.3 Å from the hydronium ion will make the process less exothermic, close to being thermoneutral. Alternatively, a positively charged amino group will render the H_2O molecule a much better acid, thus making the protonation of **2d** by H_2O thermoneutral.[53] The protein pocket is responsible for rendering the protonation process mild, neither energy demanding nor energy wasting.

The last point which is summarized in Figure 7a is the role of the thiolate in the generation of Cpd I from **2d**. Calculations show that while the removal of the thiolate still leads to a barrier-free formation of Cpd I, it decreases the proton affinity of the neutral iron(III)-OOH by 85.2 kcal/mol. If the overall process in the protein pocket is indeed close to being thermoneutral, this significant decrease of the proton affinity would prevent the protonation. It follows that the thiolate ligand plays an important role in promoting the O−O bond cleavage leading to Cpd I.

C. Ethene Epoxidation by Iron(III)-OOH. To assess the efficiency of the hydroperoxo species as an oxidant, we choose the epoxidation reaction of ethene, primarily because this reaction is viewed as a marker of **2d**.[11,16] At the outset, the data in Figure 5 rule out any reaction of **2d** by OH^+ transfer, and favor either HO• or O-atom transfer reactions. Figure 8 shows the reaction energies of the most favorable processes available to **2d** for ethene epoxidation. It is seen from the figure that the available processes involve indeed the O-atom transfer to form either a free epoxide or an iron(II)-epoxide complex. Yet another process involves epoxidation as well as self-hydroxylation of

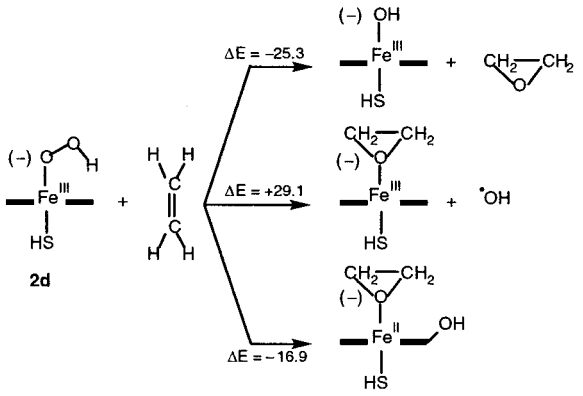

Figure 8. Reaction energies of the most favorable epoxidation processes of ethene by **2d**.

the meso carbon position of the heme. The most exothermic process in Figure 8 correponds to the formation of free epoxide, and the reaction energy is very similar to the epoxidation by Cpd I ($\Delta E = -25.3$ and -27.9 kcal/mol, respectively).[41] All the alternative processes, such as formation of the protonated epoxide by OH^+ transfer, are not shown in Figure 8 since they are highly endothermic, and they will not be considered further.

From a mechanistic point of view, the epoxidation of ethene by **2d** may occur via concerted and/or stepwise pathways, and via either the distal or the proximal oxygen atoms of **2d**. Each of these four potential energy surfaces was explored individually first by scanning (the scans are given in Supporting Information) along a chosen coordinate. Subsequently, the highest points on the scan were subjected to transition state search and to frequency characterization (see Theoretical Methods section). The main results are presented in Figures 9, 10, and 11.

The transition states for the concerted epoxidation are shown in Figure 9, along with the corresponding reaction profiles (the reactant clusters are omitted for clarity and can be found in Table S6). The proximal-attack transition state, $TS(O_p)_c$, shows the expected elongation of the C−C, O−O, and Fe−O bonds. The group spin density (ρ) data indicate an incipient OH• and almost no free spin on iron, thereby foretelling the connection of this TS to the product set, P_1, composed of Fe(II)-epoxide complex and an OH• radical. Indeed following down from the transition state leads to these products (P_1). In addition to this pathway, we identified a path along which the OH group in flight is inserted into the meso carbon of the porphine (P_2). The third possibility in which OH is inserted into the coordination sphere of the iron to give (P_3) was not observed. The two located pathways are found to coincide in the area of the transition state, $TS(O_p)_c$, in terms of geometries and energies. This suggests that $TS(O_p)_c$ might be bifurcating to two different products P_1 and P_2 as found in other processes.[54] At present, we cannot verify this feature because the size of the system prohibits IRC calculations and identification of bifurcation points by frequency projection along the path.

The distal transition state species, $TS(O_d)_c$, in Figure 9 shows activation of the O−O and C−C bonds concomitant with the shortening of the Fe−O_p bond and incipient H−O_p bonding. At the same time there is hardly any spin transfer from the iron that remains as an iron(III) center having an unpaired electron.

(53) This protonation of the reduced oxyferrous is assisted by proton hopping through the hydrogen bonding network. See: Harris, D. L.; Batista, V. S.; Miller, W. H.; Guallar, V. 12th International Conference on Cytochrome P450; La grande Motte, France, Abstract CL1-3, September 11−15, 2001. Such a process may occur also for the protonation of **2d**.

(54) (a) Bakken, V.; Danovich, D.; Shaik, S.; Schlegel, H. B. *J. Am. Chem. Soc.* **2001**, *123*, 130−134. (b) Shustov, G. V.; Rauk, A. *J. Org. Chem.* **1998**, *63*, 5413−5422.

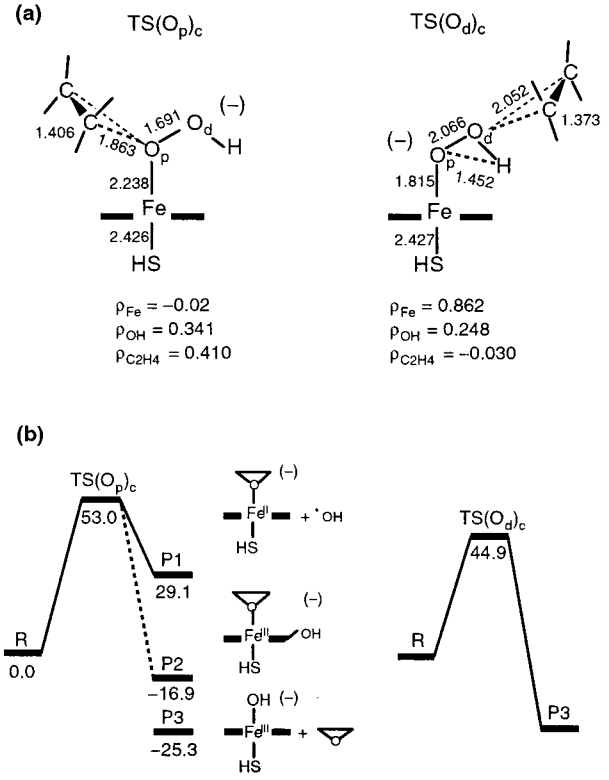

Figure 9. Transition state (TS) structures and group spin densities (ρ) in (a), and energy profiles in (b), for the concerted ethene epoxidation by **2d**. $TS(O_p)_c$ and $TS(O_d)_c$ correspond to the transition states for epoxidation by the proximal oxygen and the distal oxygen, respectively. Possible products through bifurcation are shown in dashed lines on the profile. The subscript "c" denotes "concerted". The energy figures on the profiles are in kcal/mol units.

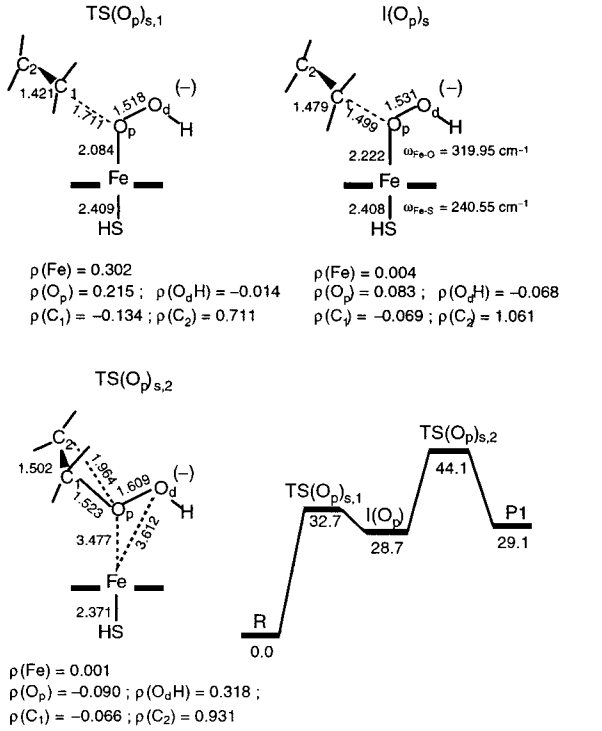

Figure 10. Structures of transition states (TS) and the intermediate (I), and the respective energy profile, for the stepwise ethene epoxidation by **2d** via the proximal oxygen. The subscript "s" denotes "stepwise". The ρ values correspond to group spin densities. The ω's are frequencies. The energy figures on the profile are in kcal/mol units.

These latter features are indicative of the fact that epoxidation occurs with concomitant migration of the hydrogen from the distal to the proximal oxygen to generate iron(III)-hydroxo and a free epoxide (P_3). Indeed, a careful analysis of the concerted distal path shows that the OH group is first inserted into ethene, then past the transition state, on the downward slope, the OH group flips, and the hydrogen atom is released toward the proximal oxygen atom of the active species.

Frequency analysis shows that the two transition states, in Figure 9, are second-order saddle points, with two imaginary modes. One mode ($\omega = i811.5$ cm^{-1} for $TS(O_p)_c$, $\omega = i1005.5$ cm^{-1} for $TS(O_d)_c$) describes the concerted motion of the atoms to form the requisite bonds, while the second mode ($\omega = i361.3$ cm^{-1} for $TS(O_p)_c$, $\omega = i146.6$ cm^{-1} for $TS(O_d)_c$) corresponds to a rotation of the ethene from a concerted two-bond formation to a single-bond formation. This feature of the concerted pathways was found also in the epoxidation of ethene by Cpd I (for which the corresponding mode frequency is $\omega = i44$ cm^{-1}).[43] Thus, oxygen-insertion is not a synchronous concerted mechanism either by Cpd I or by the putative second oxidant, iron(III)-hydroperoxo.

The stepwise mechanisms are summarized in Figures 10 and 11. Figure 10 shows the transition states and intermediate along the stepwise epoxidation by the proximal oxygen of iron(III)-hydroperoxo. The first transition state, $TS(O_p)_{s,1}$, corresponds to the bond activation of ethene, and the spin density distribution reveals this feature of the TS (imaginary frequency, $\omega = i683.5$ cm^{-1}). Thus, relative to the reactant iron(III)-hydroperoxo complex, there is a transfer of spin density from the iron center to the ethene and to the proximal oxygen. The spin density distribution in the C_2- -C_1- -O array exhibits the typical pattern of three-electron delocalization, with a negative spin density on the central moiety, C_1, flanked by positive densities on the two terminal moieties, C_2 and O_p.[40,41] In the intermediate, $I(O_p)_s$, the iron center loses virtually all the free spin, which is now localized on C_2 that becomes the new radical center. The Fe−O bond is elongated somewhat, and the distances in the OOH unit are very similar to those in the analogous iron(III)-hydrogen peroxide complex reported by Harris and Loew.[30] This intermediate follows by ring closure to yield the iron(II)-epoxide complex and OH$^\bullet$ (P_1) as products. Indeed the second transition state, $TS(O_p)_{s,2}$, exhibits an incipient epoxide ring and an elongated O−O bond (imaginary frequency, $\omega = i379.5$ cm^{-1}). The spin density distribution is also in accord with the incipient products; the free spin on the iron virtually disappears, and there is a spin density development on the leaving distal OH. The two Fe−O bond distances of the transition state show that the OOH moiety is only weakly coordinated to the iron center, and the two Fe−O distances are roughly equal. Thus, while this transition state was followed down to the set of products P_1, its geometry indicates that it may have bifurcated to P_3 (see Figure 9).

Two stepwise mechanisms for epoxidation by the distal oxygen were located. Figure 11 shows the one that possesses lower barriers.[55] Here, the bond activation leads initially to an intermediate species composed of the cluster of Cpd II and β-hydroxy ethyl radical, $I(O_d)_s$. The Fe−O and Fe−S frequencies and distances are indeed consistent with those of Cpd II. Subsequently, there could occur hydrogen atom transfer from

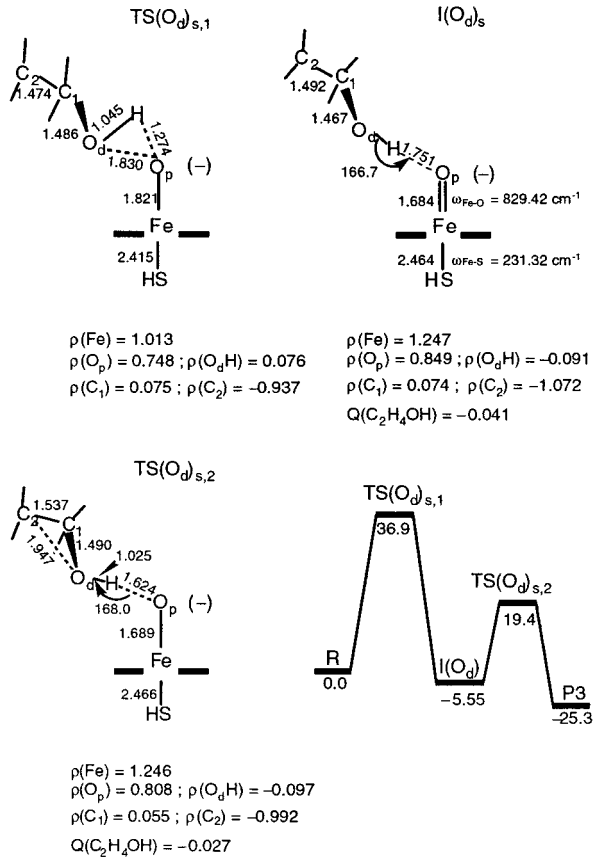

Figure 11. Structures of transition states (TS) and the intermediate (I), and the corresponding energy profile for the stepwise ethene epoxidation by **2d** via the distal oxygen. The subscript "s" denotes "stepwise". The ρ values correspond to group spin densities. The ω's correspond to frequencies. The energy figures on the profile are in kcal/mol units.

the β-hydroxoethyl radical to the oxo moiety of Cpd II, with concomitant ring closure via $TS(O_d)_{s,2}$ that leads to the products, P_3. Because we had difficulties with this latter transition state, its connection to P_3 is in fact dubious (see Theoretical Methods). Be this as it may, the bond activation step with a barrier of 36.9 kcal/mol will, in any case, be rate-limiting.

D. Comparison of the Oxidation Capabilities of Iron(III)-OOH and Cpd I. How powerful an oxidant is the iron(III)-hydroperoxo species? To answer this question, we must compare the computed barriers in Figures 9−11 to the epoxidation barriers by Cpd I computed recently in our group.[41,43] This is done in Scheme 4. It is seen that Cpd I operates as a two-state oxidant due to the proximity of its antiferromagnetic and ferromagnetic pair of ground states. The epoxidation mechanism is preferably nonsynchronous, where the high spin state gives rise to a carbon radical intermediate, which can lose stereochemistry, whereas the low spin state results in an effectively concerted epoxidation. The reactivity of iron(III)-hydroperoxo is limited to a single ground state, $^2\Pi_{yz}(Fe^{III})$.[48] However, this single state has a rich chemistry giving rise to epoxidation as well as to heme degradation. Here too, the stepwise mechanisms are preferred over the concerted ones, as for Cpd I. However, the relative barriers show a great difference between the two oxidants. While Cpd I is a powerful epoxidant with very low barriers, the iron(III)-hydroperoxo species is expected to be a sluggish oxidant, if at all, since its barriers are huge. Thus, unless DFT gives very wrong results, which to the best of our knowledge is seldom the case, we must conclude that the iron(III)-hydroperoxo species of P450 by itself is not an oxidant, since it is in fact a rather strong base. It is not unlikely that proton assistance will activate the oxidative capability of iron(III)-hydroperoxo, as implied in the self-hydroxylation of the heme in HO-1.[23] However, the source and mechanism of such putative protonation remain unclear at the present and will have to await a future study.

(55) Another pathway for epoxidation through the distal oxygen was located at a somewhat higher energy (with barrier of 42 kcal/mol). This pathway has a single transition state and corresponds to a nonsynchronous but effectively concerted mechanism, during which the ethene is activated, the O−O bond is cleaved, the epoxide ring is formed, and the hydrogen of the distal oxygen migrates to the proximal oxygen to give product set, P_3. This behavior makes good sense because bonding of the ethene to the distal oxygen behaves like the corresponding protonation (Figure 1) and leads to a barrier-free O−O bond breaking. All these events transpire past the transition states, en-route to the product.

Scheme 4. Barriers and Mechanistic Features of Epoxidation by Cpd I and by **2d**[a]

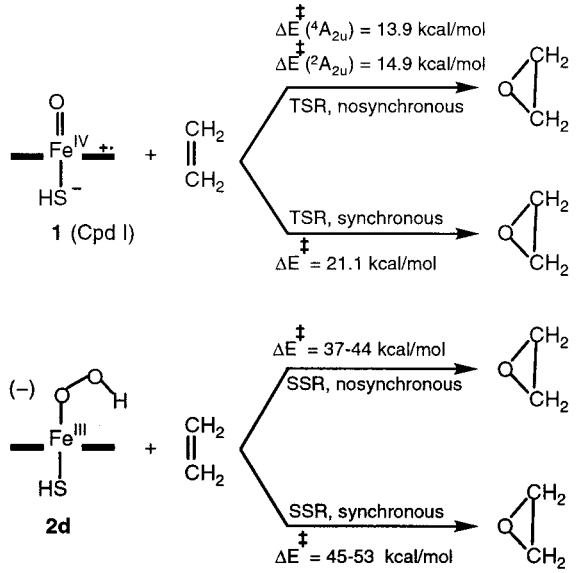

[a] Cpd I exhibits two state reactivity (TSR) with low barriers, while **2d** exhibits a single state reactivity (SSR) with very large barriers.

IV. Conclusions

The present paper addresses the electronic structure of iron(III)-hydroperoxo and its potential reactivity as an oxidant. Its oxidative capability is studied with reference to olefin epoxidation that is considered to be the marker reaction for this putative oxidant. The theoretical results show that the species is a fairly strong base (or nucleophilic in other words) with a significant proton affinity, and its ability to accept an additional electron density is rather poor (see data in Figure 6), even poorer than that of Cpd II which is known to be a sluggish oxidant (see note added in proof; ref 65). In accord with that, the four possible ethylene epoxidation pathways (Figures 9−11) exhibit barriers that range between 37 and 53 kcal/mol. These barriers are much higher than the corresponding ones for ethylene epoxidation by Compound I (14 kcal/mol). The conclusion from this study is straightforward: $Fe(III)\text{-}OOH^{(-)}$ cannot be an oxidant as such. While these results suggest, at face value, that P450 uses a single oxidant, viz. Compound I, we must be attentive. We suggest that a second oxidant has to be searched elsewhere in the catalytic cycle as well as among the dioxygen

wasting ("uncoupling") processes. We plan to look for other candidates among the species in Scheme 2.

V. Theoretical Methods

Model Systems. The heme site of the active species of P450 consists of an iron protorporphyrin IX, connected to the apoprotein by an Fe−S(Cys) linkage. Our calculations excluded the ring substituents since these substituents were found to have a negligible effect,[36] and since their presence will have made this study impossible. Thus, the model species used in the study have the general formula ([(SH)Fe(Porphine)-(distal ligand)] (distal ligand = O, OH, OH_2, etc.).

The use of HS rather than a mercaptide (SCH_3)[47a−g] group as a proximal ligand merits a comment. First, this choice does not affect the conclusions of the study. Thus, in a previous paper[41] it was demonstrated that the salient features of ethylene epoxidation by a Cpd I model that involved HS as a ligand did not change when the ligand was replaced by a mercaptide. Here too, our results for **2d** are virtually identical to those of Harris and Loew[30] who used mercaptide as a ligand. Second, we try to stick to models which are uniformly good for all the species of the enzyme. Thus, it is our experience with Cpd I that by criteria of electron affinities, bond energy, spin densities, and states ordering, HS is a more suitable model for the SCys ligand.[34,40] For example, our calculated (B3LYP/6-311++G**) electron affinities are (in kcal/mol) HS (54.0), SCys (60.2), and SCH_3 (42.9). Apparently, the cysteinato ligand in its most stable conformation, which involves internal NH- - -O═C and NH- - -S hydrogen bonds, has an electron affinity closer to HS, and much higher than SCH_3. These internal hydrogen bonds mimic, in part, some of the interactions in the cysteine helix within the protein pocket[56,57] (i.e., three NH- - -S hydrogen bonds with Leu_{358}, Gly_{359}, and Glu_{360}, and NH- - -O═C with e.g., Phe_{350}). There exists yet another conformation of SCys devoid of these internal hydrogen bonds.[47f] This conformation lies ca. 20 kcal/mol higher in energy and has a low electron affinity, leading to a Cpd I species with almost pure sulfur radical character and no porphyrin radical cation character.[47f] Had Cpd I been like that it would have appeared red instead of green.[7] The fact that Cpd I of CPO (that has a SCys proximal ligand) is green[58] and not red is a strong indication of a significant porphyrin cation radical.

Technical Details. The computational details are similar to those of our previous computational studies in the P450 field.[33−43] The study was carried out with density functional theory (DFT). Calculations were done with the JAGUAR 4.1 package[59] using wherever possible both restricted (RODFT) and unrestricted (UDFT) hybrid functional, B3LYP.[60,61]

A double-ζ quality basis set was used, employing 6-31G for C, H, N, S, and O, and LACVP[62] coupled with the Los Alamos effective core potential for Fe. This LACVP(6-31G) basis set has proven qualitatively reliable[33,34] and of similar performance to higher level basis sets.[34−36] Some tests with the triple-ζ quality basis set augmented with diffuse and polarization functions, LACV3P+*, were done here too on the electron affinities, protonation, and extrusion reactions (Figures 5−7), with no change in the results and conclusions derived from the LACVP (6-31G) basis set. The LACV3P+* data are shown in the last section of the Supporting Information.

Solvent calculations were carried out with the iterative polarized continuum model (PCM) as implemented in JAGUAR 4.1.[59,63] A dielectric constant $\epsilon = 5.7$ corresponding to chlorobenzene as a solvent was used (the program specifies the dielectric constant, $\epsilon = 5.7$, and the probe radius of the solvent, $r = 2.722$ Å).

Fully converged species with JAGUAR are exported to the GAUSSIAN98 program[64] for frequency analyses. GAUSSIAN computes analytical frequencies which are considerably less time-consuming than those with JAGUAR.

Strategy of Calculation. This work is divided in two parts. In the first part, the title complex, $[PorSHFeOOH]^{-1}$ (**2d**) is characterized and compared to some relevant species, to assess its "electrophilicity". This requested a large amount of work on related species such as $[PorSHFeOOH]^{0,-2}$ ($\mathbf{2d}^{+1,-1}$), $[PorSHFeOOH]^{-1}$ (**2p**), [PorSHFeO] (Cpd I, **1**), $[PorSHFeO]^{-1}$ (Cpd II, $\mathbf{11} = \mathbf{1}^{-1}$), $[PorSHFeO]^{-2}$ (Cpd III, $\mathbf{1}^{-2}$), $[PorSHFeOH]^{0,-1,-2}$ (**12**), $[PorFeO]^{1,0,-1}$ (**13**), $[PorFeOOH]^{+1,0,-1}$ (**14**), $[PorSHFeOH_2]$, etc. All these species were fully optimized without any symmetry constraints at the UB3LYP/LACVP-6-31G level of theory and characterized for several spin situations and configurations. This results in original characterization and description of more than 50 new states. The details of most of these states are given in Tables S1−S5 of the Supporting Information.

The second part is devoted to the study of ethylene epoxidation by **2d**.[48] We investigated four processes corresponding to stepwise and concerted attacks of the ethene on each of the two oxygen atoms of the hydroperoxo ligand of **2d**. The general procedure we used can be described as follows: The potential energy surfaces (EPS) are explored using a scanning technique with very fine steps, to establish the connection between reactants to a specific set of products. Many different scans were explored, and the lowest energy ones provided the basis for Figures 9−11. These scans are detailed in the Supporting Information. Caution was exercised during the scans to ascertain that the calculations followed the lowest energy surface and that there was no surface crossing or bifurcation along the scan. This was done by swapping orbitals and testing other electronic solutions throughout the scan. These test calculations were carried out at the RODFT level, except for the case of the stepwise attack on the distal oxygen atom (Figure 11) for which the nature of the intermediate (a doublet triradicaloid) required the use of the UDFT formalism. Subsequently, all the critical points of the surfaces, minima, and transition states (TS) were fully optimized at the UDFT level of theory and finally characterized by frequency analysis.

Location of the transition states (TS's) of this study involves inherent difficulties, due to the high energy of the species and because of the complex motions inherent in the transition state modes (e.g., Figure 11). In most of the TS's we were able to overcome the difficulties. Two transition states, $TS(O_p)_{s,2}$ and $TS(O_d)_{s,1}$, encountered convergence difficulties in the geometry optimization, due to soft motions such as internal rotations. Because the scans were done with very fine steps, the extrema of the scans give reliable estimates of the barriers, and the geometries corresponding to the extrema of the respective scans were used as the TS's. The frequency analyses of these structures were carried out to confirm that this approximation was acceptable. Both structures

(56) Poulos, T. L. *J. Bioinorg. Chem.* **1996**, *1*, 356−359.
(57) Poulos, T. L.; Vickery, J. C.; Li, H. In *Cytochrome P450: Structure, Mechanisms and Biochemistry*, 2nd ed.; Ortiz de Montellano, P. R., Ed.; Plenum Press: New York, 1995; Chapter 4.
(58) Hosten, C. M.; Sullivan, A. M.; Palaniappan, V.; Fitzgerald, M. M.; Terner. J. *J. Biol. Chem.* **1994**, *269*, 13966−13978.
(59) *JAGUAR 4.1*; Schrödinger, Inc.: Portland, OR, 2000.
(60) Stevens, P. J.; Devlin, F. J.; Chablowski, C. F.; Frisch, M. J. *J. Phys. Chem.* **1994**, *98*, 11623−11627.
(61) Becke, A. D. *J. Chem. Phys.* **1993**, *98*, 5648−5652; **1992**, *96*, 2155−2160; **1992**, *97*, 9173−9177.
(62) LACVP basis set is derived from LAN2DZ: Hay, J. P.; Wadt, W. R. *J. Chem. Phys.* **1985**, *82*, 299.
(63) See, for example: Marten, B.; Kim, K.; Cortis, C.; Friesner, R. A.; Murphy, R. B.; Ringnalda, M. N.; Sitkoff, D.; Honig, B. *J. Phys. Chem.* **1996**, *100*, 11775−11788.
(64) Frisch, M. J.; Trucks, G. W.; Schlegel, H. B.; Scuseria, G. E.; Robb, M. A.; Cheeseman, J. R.; Zakrzewski, V. G.; Montgomery, J. A., Jr.; Stratmann, R. E.; Burant, J. C.; Dapprich, S.; Millam, J. M.; Daniels, A. D.; Kudin, K. N.; Strain, M. C.; Farkas, O.; Tomasi, J.; Barone, V.; Cossi, M.; Cammi, R.; Mennucci, B.; Pomelli, C.; Adamo, C.; Clifford, S.; Ochterski, J.; Petersson, G. A.; Ayala, P. Y.; Cui, Q.; Morokuma, K.; Malick, D. K.; Rabuck, A. D.; Raghavachari, K.; Foresman, J. B.; Cioslowski, J.; Ortiz, J. V.; Stefanov, B. B.; Liu, G.; Liashenko, A.; Piskorz, P.; Komaromi, I.; Gomperts, R.; Martin, R. L.; Fox, D. J.; Keith, T.; Al-Laham, M. A.; Peng, C. Y.; Nanayakkara, A.; Gonzalez, C.; Challacombe, M.; Gill, P. M. W.; Johnson, B. G.; Chen, W.; Wong, M. W.; Andres, J. L.; Head-Gordon, M.; Replogle, E. S.; Pople, J. A. *Gaussian 98*; Gaussian, Inc.: Pittsburgh, PA, 1998.
(65) Note added in proof; see similar conclusions in: Meunier, B.; Bernadou, J. *Struct. Bonding* **2000**, *97*, 1−36.

were found to exhibit the expected single imaginary frequency. TS-$(O_d)_{s,2}$, on the other hand, did not pass the frequency test and is perhaps not a good approximation of the actual TS. This may be associated with the complexity of the reaction coordinate of this TS that accounts for the formation of the C−O bond, for the cleavage of the O_d−H bond, and for the formation of the O_p−H bond. The optimization of this very complex coordinate, especially for a big system as in the present study, is still a difficult task. Thus, while the TS followed down to the geometry corresponding to P_3, the electronic structure still did not reflect the OH bond interchange. Fortunately, $TS(O_d)_{s,2}$ is not associated with the rate-limiting step of this process leaving the overall mechanistic picture unaltered. A perfectly characterized pathway mentioned in ref 55 gave a higher barrier of 42 kcal/mol and was therefore excluded in favor of the mehcanism in Figure 11. Clearly, therefore, the quality of $TS(O_d)_{s,2}$ does not affect the basic conclusions of this paper, that **2d** is not a good oxidant due to its electron richness and high basicity.

Acknowledgment. This paper is dedicated in memoriam of G. H. Loew, a pioneer in P450 theoretical research. The research is supported in part by the Israel Science Foundation (ISF), the German-Israeli Binational Foundation (GIF), and by the Ministry of Science, Culture, and Sport. F.O. thanks the European Union for a Marie Curie Fellowship.

Supporting Information Available: Six tables with properties of all the species mentioned in the text and scans of epoxidation pathways (PDF). This material is available free of charge via the Internet at http://pubs.acs.org.

JA0171963